ADVANCED FUNCTIONAL MATERIALS
www.afm-journal.de

Optimization of the Power Conversion Efficiency of Room Temperature-Fabricated Polymer Solar Cells Utilizing Solution Processed Tungsten Oxide and Conjugated Polyelectrolyte as Electrode Interlayer

*Lie Chen, Chen Xie, and Yiwang Chen**

The utilization of a conjugated polyelectrolyte-ionic liquid crystal (CPE-ILC) complex as electron transporting layer (ETL) to improve the compatibility between the ITO and hydrophobic active layer and to promote the dipole orientation at cathode interface is reported. Simultaneously, a hole transporting layer (HTL) of solution processed tungsten oxide together with poly(2,6-bis(trimethyltin)-4,8-bis(5-(2-ethylhexyl)thiophen-2-yl)benzo[1,2-b:4,5-b′]dithiophene-alt-4,6-Dibromo-thieno[3,4-b]thiophene-2-carboxylic acid 2-[2-(2-methoxy-ethoxy)-ethoxy]-ethyl ester) (PBDTT-TT-TEG) efficiently shifts the work function of Ag electrode in this device. The interfacial modification of these interlayers achieves energy alignment at both electrodes. The power conversion efficiency (PCE) of the PSC based on ITO/PFN-CbpSO/PBDTTT-C-T:$PC_{70}BM$/PBDTT-TT-TEG/WO_3/Ag with solution processed interlayers reaches to 7.8%. It is worthy to note that except for the electrodes, all layers of device are fabricated by solution process at room temperature and without annealing. In the case of incorporating ZnO layer into this device, the device efficiency further increases to 8.5%, which is the best value reported from PBDTTT-C-T:$PC_{70}BM$-based solar cells with solution processed interlayers at both electrodes so far.

1. Introduction

Polymer solar cells (PSCs) based on the bulk heterojunction (BHJ) blend of a conjugated polymer donor and a fullerene acceptor have gained considerable attentions as a cost-efficient, flexible, and portable energy source.[1–3] The research field of PSCs has diversified into at least three overlapping fractions: high power conversion efficiency (PCE), stability and the compatibility to the printing or roll-to-roll technique.[4,5] Today, the main topic is still on PCE improvement through design of novel light-harvesting polymers, usage of efficient device structures, development of new fabrication techniques and incorporation of interfacial materials for electrode modification.[6–14] This progress of stability has been gained by the inverted device structures of the bulk heterojunction geometry, which allows for more stable metal electrodes, the choice of more photostable active materials and the introduction of interfacial layers.[11,13,15–17] Roll-to-roll solution processing of PSCs is widely considered as one of the key technologies towards commercialization of photovoltaic devices.[18–21] High PCE, long-term stability and solution processing thus are the most crucial considerations for achieving commercialization of PSCs.

For a specific solution processed PSC with high performance, one of the biggest challenges is the design of reliable, environmental robust and easily processable charge-selective layers. These layers that are typically processed between the semiconductor and the electrode can selectively extract one type of carrier, while the other type of carrier is rejected by a barrier or counter field induced by an energy mismatch. The commonly used conductive polymer blend for solution processed devices, poly(3,4-ethylenedioxythiophene):poly(styrenesulfonate) (PEDOT:PSS), is not an optimum hole transporting layer (HTL) due to its hygroscopicity and acidity, which negatively impacts the environmental stability of PSCs.[5,22,23] Promising replacements and currently heavily investigated substitutes for PEDOT:PSS come from the class of transition metal oxides (MO), including MoO_3,[24–29] V_2O_5,[29–32] NiO,[33–35] SbO_3,[36] and WO_3.[37–44] PSCs using such layers showed comparable efficiencies to those using the PEDOT:PSS layer. Moreover, they are advantageous over the PEDOT:PSS layer since they are neutral, chemically stable, and photo-stable. Significant progress was also reported for electron transporting layer (ETL) based on MOs, such as $CsCO_3$, TiO_x, and ZnO.[15,45–49] The traditional approach for MO transition is through evaporation in high vacuum. The need for solution processed MO gave rise to a comprehensive development of precursor processes for transition MO layers. Unfortunately, most MO formations take place at high temperatures and under ambient conditions since this process requires the presence of either oxygen or water.[50] This is in conflict with the particular requirements for PSCs fabrication where, as of today, inert and room temperature processing is necessary for device life-times and printability.

Prof. L. Chen, C. Xie, Prof. Y. Chen
Institute of Polymers/Department of Chemistry
Nanchang University
999 Xuefu Avenue
Nanchang 330031, China
E-mail: ywchen@ncu.edu.cn

DOI: 10.1002/adfm.201304256

To circumvent the inherent weaknesses of the MO interlayers, organic interfacial materials have also been employed into cathode, such as conjugated polyelectrolytes (CPEs),[51–53] nonconjugated polymers[54–56] and fullerene derivatives.[57–62] Because of the ionic nature of the side chain, organic interlayers are soluble in typical polar solvents and form permanent dipole moments at the cathode/active layer interface to facilitate charge dissociation, injection and collection. The organic/polymeric interlayers also can offer better compatibility in device fabrication by facile room temperature processing from organic solvents.

In this work, through interfacial modification by conjugated polyelectrolyte-ionic liquid crystal (CPE-ILC) ETL and low surface energy polymer/WO_3 HTL, a room temperature solution processed inverted PSC (I-PSC) based on poly(4,8-bis(5-(2-ethyl-hexyl)-thiophene-2-yl)-benzo[l,2-b:4,5-b′]dithiophene-alt-alkylcarbonyl-thieno[3,4-b]thiophene)[63] PBDTTT-C-T:$PC_{70}BM$ active layer with high efficiency, solution processibility and long-term air stability have been developed (**Figure 1**). A stable CPE-ILC PFN-CbpSO complex is produced by mixing an anionic ILC sodium 4-(4′-cyano-biphenyl-4-yloxy)-butane-1-sulfonate (CbpSO-Na) with the classical CPE poly[(9,9-bis(6′-(*N*,*N*,*N*-trimethylammonium)hexyl)-2,7-fluorene)-alt-2,7-(9,9-dioctylfluorene)] (PFN-Br) with cationic side chains via the electrostatic attraction. The self-assembled CPE-ILC complex as ETL is not only compatible with hydrophobic active layer, but also rearranges the orientation of dipole moments at cathode interface. For the HTL, the WO_3 was deposited from tungsten(V) ethoxide ($W(OEt)_5$) or tungsten(VI) ethoxide ($W(OEt)_6$) precursor solution at room temperature. Moreover, incorporation of a small amount of the low surface energy polymer poly(2,6-bis(trimethyltin)-4,8-bis(5-(2-ethylhexyl)thiophen-2-yl) benzo[1,2-b:4,5-b′]dithiophene-alt-4,6-Dibromo-thieno[3,4-b] thiophene-2-carboxylic acid 2-[2-(2-methoxy-ethoxy)-ethoxy]-ethyl ester) (PBDTT-TT-TEG) with ter(ethylene glycol) (TEG) side chains into PBDTTT-C-T:$PC_{70}BM$ blend induces a spontaneous vertical phase separation with formation of PBDTT-TT-TEG buffer layer on the top of the active layer. The self-organized polymer PBDTT-TT-TEG not only improves the adhesion between the active layer and solution processed WO_3 (sWO_3) precursor solution, but also can increase the work function of anode for better energy alignment. By using the relatively non-hygroscopic CPE-ILC PFN-CbpSO and PBDTT-TT-TEG/sWO_3 instead of traditional CPE and PEDOT:PSS as interlayer, an optimized PCE of the solution processed PSC has surpassed 7.8% together with improved device stability in air. It is worthy to note that except for the electrodes, all layers of the device are fabricated by solution process at room temperature and without annealing. Introduction of a layer of solution processed ZnO into the device can further improve the PCE to 8.5%. To the best of our knowledge, this is the best PCE value for PBDTTT-C-T:$PC_{70}BM$-based solar cells with solution processed interlayers reported to date.

2. Results and Discussion

PFN-CbpSO complex was prepared from CPE PFN-Br with the ILC CbpSO-Na (Figure 1). The PFN-Br was synthesized according to our previous work.[64] The CbpSO-Na is used as the counterpart to mix with the cationic PFN-Br at a molar ratio of 1:2 (PFN-Br:CbpSO-Na). Although both PFN-Br and CbpSO-Na are water-soluble, a light yellow precipitate formed as soon as stoichiometric amounts of PFN-Br and CbpSO-Na were mixed in water. This is ascribed to the electrostatic assembly between the cationic moieties in PFN-Br and anionic moieties in CbpSO-Na, resulting in the polymer backbones surrounded by nonpolar alkyl side chains.[65] The precipitates were then collected, washed with de-ionized water to remove the residual water-soluble compounds and salts, and finally dried in vacuum to yield the stoichiometric PFN-CbpSO complex with confirmed structure (Figure S1, Supporting Information). To check the effect of the ILC content on the electrostatic assembly between PFN-Br and CbpSO-Na, PFN-CbpSO complex with the molar ratio of 1:1 (PFN-Br:CbpSO-Na) was also prepared for comparison. The PFN-CbpSO complexes have good solubility in methanol and DMSO, which ensures the environmental solution processibility.

Figure S2 (Supporting Information) demonstrates the UV-vis absorption spectra and PL spectra of the PFN-Br and PFN-Br:CbpSO-Na complex with the molar ratio of 1:1 and 1:2. Both of the PFN-CbpSO complexes give red-shift bands with respect to the pristine PFN-Br film, suggesting that ILC CbpSO-Na can favor the more oriented backbone induced by the electrostatic assembly between the cationic PFN-Br and anionic CbpSO-Na. Thus, the stoichiometric PFN-CbpSO complex (1:2) shows the more obvious red-shift band than the partly assembled PFN-CbpSO complex (1:1). The increased electronic delocalization from the improved planarization of the backbone can be also confirmed by the PL spectra of the PFN-Br and PFN-Br:CbpSO-Na complex, as shown in Figure S2 (Supporting Information), where similar red-shifted emitting bands can be observed from the ILC modified CPE, especially from the stoichiometric counterpart.

The CPE-ILC complex film with the liquid crystal-induced ordered polar chains is preferable to form an aligned dipole moment at metal/organic material interface. **Figure 2** presents work function (WF) results of the CPE-covered indium-tin-oxide (ITO) electrodes through ultraviolet photoelectron spectroscopy (UPS) measurement, and the full UPS profiles are shown in Figure S3 (Supporting Information). For the measurements, thin CPE films with a thickness of approximately 10 nm were cast from methanol solutions on the top of ITO/glass substrates. Although the reported WF value of ITO is varied from 4.7 to 5.1 eV,[11] which may be caused by the presence of environmental contaminants (such as water, O_2 or CO_2),[66] the WF value of 4.93 eV measured for the as-received ITO surface is in agreement with the literature.[67] The secondary cutoff of the PFN-Br-covered ITO electrodes successfully shifts to the higher binding energy, indicating a decrease in the effective WF of the ITO electrode to 4.24 eV (Table S1, Supporting Information). The interfacial dipole formation at ITO/PFN-Br interface can lower the Schottky barrier that is found to hamper the efficient electrons collection from the photoharvest layer to ITO. However, spin-coating a layer of PFN-CbpSO onto the ITO further reduces the WF to 4.14 eV. Since the dipole of CPE layer is determined by the ionic chain orientation, the self-assembled CPE-ILC film with ordered polar chains is

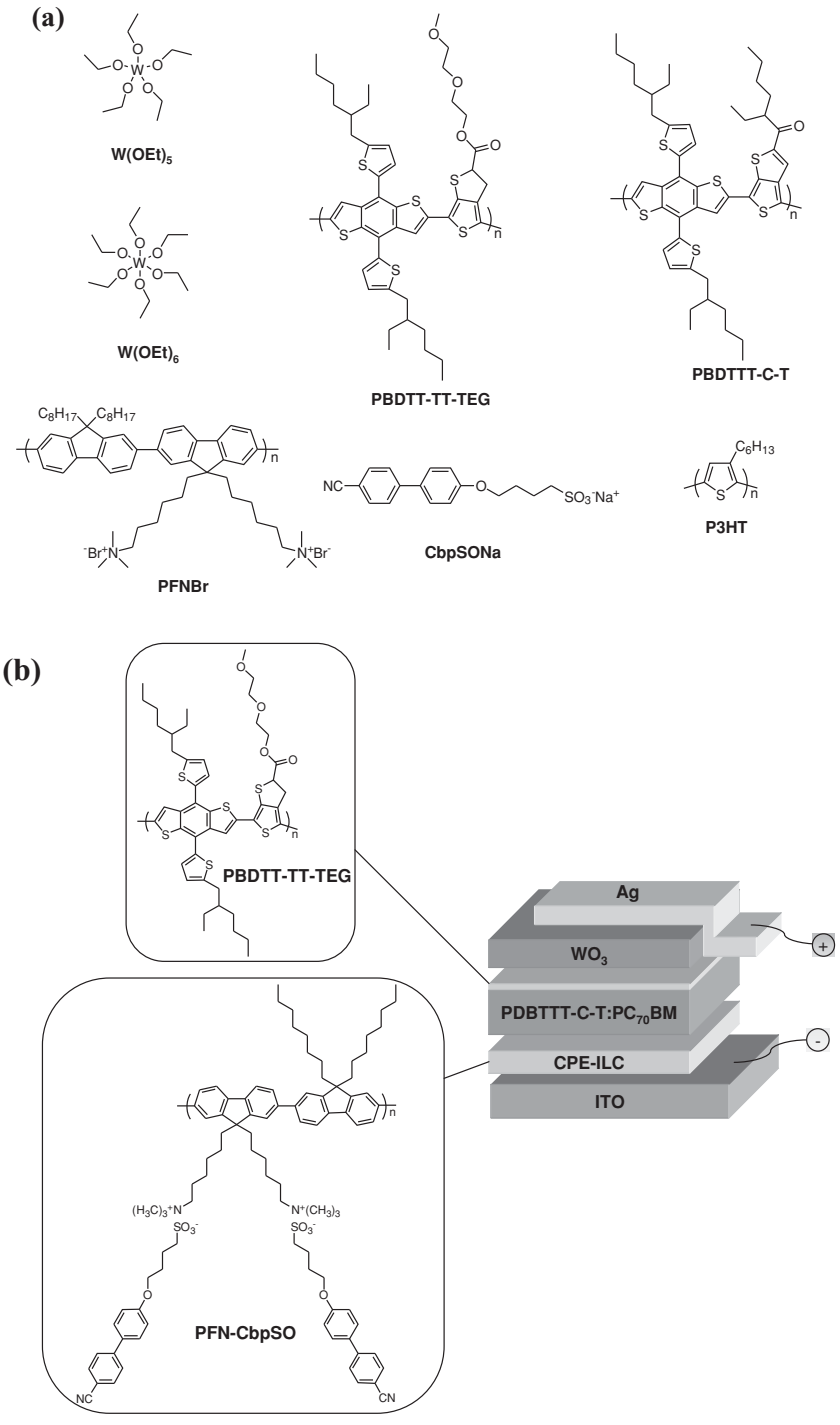

Figure 1. a) Chemical structures of the materials used for processing ETL, HTL and photoactive layer in the I-PSCs: WO_3 precursors $W(EtO)_5$, $W(EtO)_6$ and polymer PBDTT-TT-TEG for HTL; conjugated polyelectrolyte PFNBr and ionic liquid crystal CbpSONa for ETL; polymer PBDTTT-C-T and P3HT as donor for photoactive layer. b) Device structure of I-PSCs, in which the active layer is sandwiched between PFN-CbpSO complex modified ITO cathode and top Ag anode with self-assembled PBDTT-TT-TEG and solution processed WO_3 buffer layer.

preferable to form a more aligned dipole moment, which would favor a better energy alignment and form an ohmic contact at the ITO/active layer interface.[54] Therefore, the origin behind the downshift WF comes from the enhanced orientation of dipole moment caused by the LC induced polar chains orientation in CPE at the ITO/polymer interface. Photovoltaic characteristics were investigated for the inverted PSCs with Device A architectures of ITO/ETL/PBDTTT-C-T:$PC_{70}BM$/WO_3/Ag based on these ETL materials with the evaporated WO_3 (eWO_3) and Ag as the top anode. As shown in Figure 2 and **Table 1**, the average PCE of the Device A with the ITO/PFN-CbpSO cathode is dramatically improved to 7.17%, which is approximately 350% and 10% enhancement over those of the devices without ETL and with pure PFN-Br as ETL, respectively. The drastic improvement in the PCE together with J_{SC} of the devices based on the CPE-ILC ETL is attributed to the eliminated energy barrier at cathode interface and the improved capability of the electron collection of ITO achieved by the formation of highly orientated permanent dipole at ITO/active layer interface. The improved J_{SC} is may also partly related to the more imitated contact between PFN-CbpSO and the active layer. As shown in Figure S4 (Supporting Information), the water contact angle of ETL changes from 68° to 100° after adding the ILC to CPE layer, verifying the more hydrophobic film can favor a better contact with upper active layer.

For the further performance improvements, the anode interfacial engineering was also investigated. It has been reported that the addition of small amount of TEG-substituted materials in BHJ blend induces spontaneous vertical phase separation with formation of a thin layer with TEG on top of the P3HT/PCBM.[57,68] Inspired by this, a novel polymer PBDTT-TT-TEG with the identical backbone to the donor polymer PBDTTT-C-T and the TEG-substituted side chains is doped into BHJ layer. The polymer PBDTT-TT-TEG was synthesized according to the reported literatures.[63,69] It is expected that PBDTT-TT-TEG molecules can spontaneously migrate to the surface of the PBDTTT-C-T:$PC_{70}BM$ layer to form a buffer layer between the active layer and the metal anode, due to the reduced surface energy caused by TEG side chains. To investigate the surface segregation of PBDTT-TT-TEG during spin coating, X-ray photoelectron spectroscopy (XPS) was carried out (Figure S5, Supporting Information). The films were prepared on ITO-coated glass substrates by spin coating the solutions with various concentrations of TEG-caped polymer and a fixed concentration of PBDTTT-C-T at 10 mg mL^{-1}. For effective segregation of the polymer on the top of the active layer, the liquid film was dried by slowly vaporizing the solvent in inert condition. As

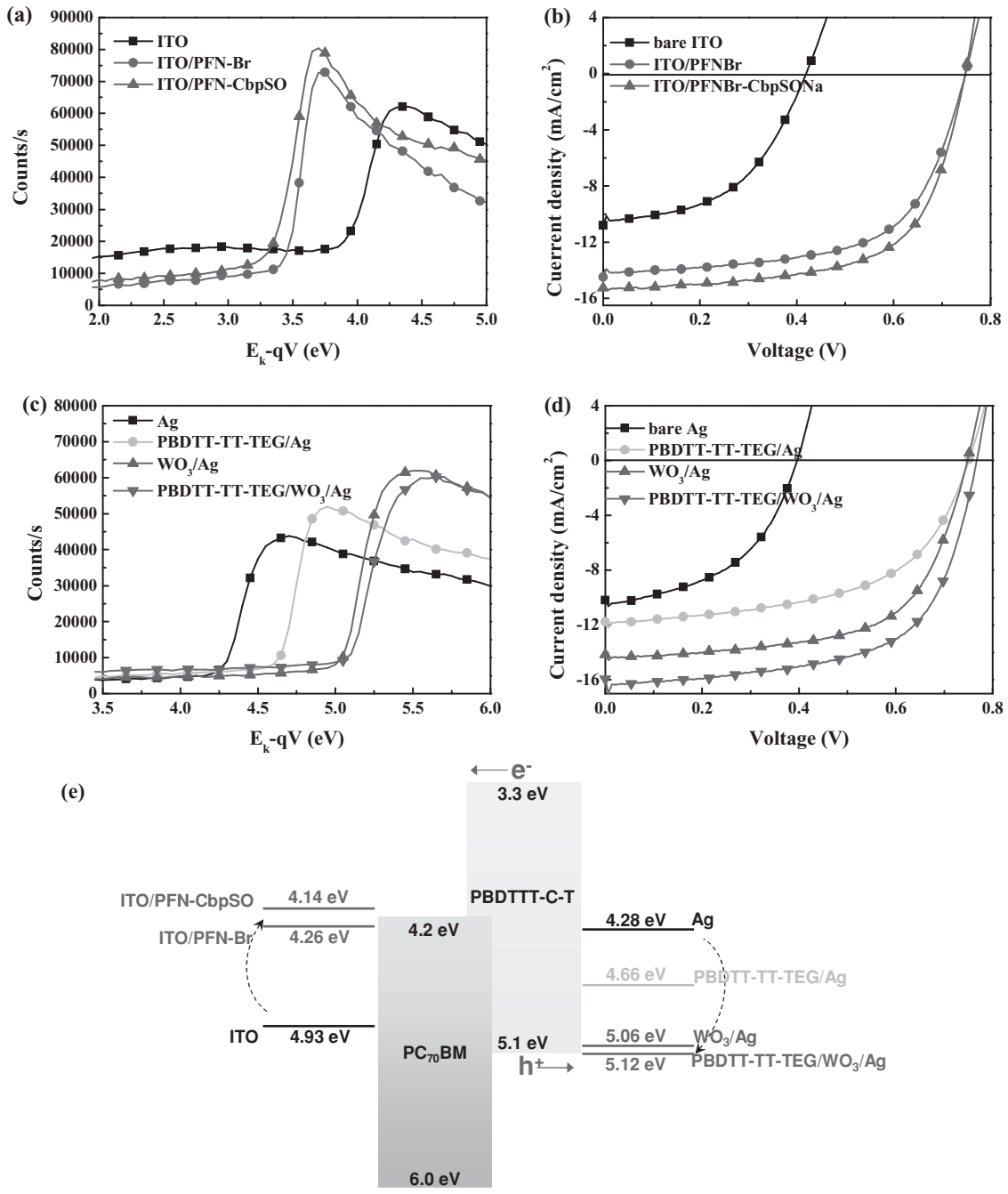

Figure 2. a) The UPS cut-off of ITO substrates with PFN-Br, PFN-CbpSO layer or without film on top; b) *J–V* characteristics of the PBDTTT-C-T:$PC_{70}BM$ inverted solar cells with cathode of ITO, ITO/PFN-Br or ITO/PFN-CbpSO; c) The UPS cut-off of thin Ag film coated on the surface of glass substrate with solution processed PBDTT-TT-TEG, WO_3, PBDTT-TT-TEG/WO_3 or without film; d) *J–V* characteristics of the PBDTTT-C-T:$PC_{70}BM$ inverted solar cells with anode of Ag, PBDTT-TT-TEG/Ag, WO_3/Ag or PBDTT-TT-TEG/WO_3/Ag; e) Schematic energy level diagram of the different investigated electrode interlayers.

shown in Figure S5 (Supporting Information), the peak of O 1s on the surface of pure PBDTTT-C-T film is attributed to the carbonyl side chains. More importantly, the surface O/C ratios of the films calculated from the peak intensities (O 1s/C 1s) are higher than those calculated from compositions ratio of the mixed solution for all concentrations. The remarkable increased O/C ratio indicates the spontaneous segregation of PBDTT-TT-TEG on the film surface during slow drying process, due to the reduced surface energy. As the concentration of polymer rises to 15 wt%, the O/C atomic ratio reaches to 7.3% and shows a signal of saturation, which means the surface of the polymer layer can be completely covered by PBDTT-TT-TEG as long as further increasing the polymer concentration.

Table 1. Summary of the photovoltaic performance of inverted PBDTTT-C-T:$PC_{70}BM$ solar cells with various interlayer.

Device[a)]	HTL[f)]	V_{OC} [V]	JSC [mA cm^{-2}]	FF [%]	average PCE [%][i)]	best PCE [%]	R_s [Ω cm^2]	R_{sh} [Ω cm^2]
control 1[b)]	eWO_3	0.42	10.0	48.5	2.04	2.18	10.1	261
control 2[c)]	eWO_3	0.75	14.2	61.0	6.50	6.58	11.8	585
A	none	0.40	10.0	47.5	1.90	2.00	15.3	165
A	PEDOT:PSS	0.73	11.9	54.0	4.69	4.90	65.7	285
A	sWO_3[g)]	0.75	14.4	58.3	6.30	6.53	11.0	638
A	sWO_3[h)]	0.75	14.2	60.5	6.44	6.70	16.5	716
A	eWO_3	0.75	14.9	64.2	7.17	7.31	43.4	1515
B	none	0.75	10.8	53.6	4.34	4.66	4.91	3.83
B	PEDOT:PSS	0.77	13.2	61.2	6.22	6.46	4.93	441
B	sWO_3[g)]	0.77	15.2	63.2	7.39	7.70	14.7	540
B	**sWO_3[h)]**	**0.77**	**15.2**	**64.2**	**7.51**	**7.82**	**2.54**	**339**
B	eWO_3	0.77	15.3	64.4	7.59	7.96	1.62	451
C control 1[d)]	eWO_3	0.75	15.1	61.1	6.92	7.18	15.4	669
C control 2[e)]	eWO_3	0.76	16.1	61.9	7.57	7.93	2.10	550
C	sWO_3[g)]	0.77	16.1	64.4	7.98	8.33	11.4	393
C	sWO_3[h)]	0.77	16.2	65.3	8.14	8.49	8.88	4889
C	eWO_3	0.77	16.2	65.8	8.21	8.53	8.18	393

[a)]Device A: glass/ITO/**PFN-CbpSO**/PBDTTT-C-T:$PC_{70}BM$ (1:1.5 w/w)/HTL/Ag; Device B: glass/ITO/PFN-CbpSO/PBDTTT-C-T:$PC_{70}BM$/**PBDTT-TT-TEG** (1:1.5:0.3 w/w)/HTL/Ag; Device C: glass/ITO/**ZnO**/PFN-CbpSO/PBDTTT-C-T:$PC_{70}BM$:PBDTT-TT-TEG/HTL/Ag. [b)]Device configuration: glass/ITO/PBDTTT-C-T:$PC_{70}BM$/HTL/Ag. [c)]Device configuration: glass/ITO/PFN-Br/PBDTTT-C-T:$PC_{70}BM$/HTL/Ag. [d)]Device configuration: glass/ITO/ZnO/PBDTTT-C-T:$PC_{70}BM$:PBDTT-TT-TEG/HTL/Ag. [e)]Device configuration: glass/ITO/ZnO/PFN-Br/PBDTTT-C-T:$PC_{70}BM$:PBDTT-TT-TEG/HTL/Ag. [f)]eWO_3: evaporated WO_3, sWO_3: solution processed WO_3. [g)]The WO_3 fabricated from $W(EtO)_5$. [h)]The WO_3 fabricated from $W(EtO)_6$. [i)]All the PCE were averaged over 5 cells. The bold value is the best performance for the room temperature-fabricated devices with solution processed electrode interlayer.

Through both cathode and anode interfacial modification by PFN-CbpSO and PBDTT-TT-TEG, performance improvement would be achieved. The *J–V* characteristics of the Devices B ITO/PFN-CbpSO/PBDTTT-C-T:$PC_{70}BM$:PBDTT-TT-TEG/Ag with PBDTT-TT-TEG as HTL and PFN-CbpSO as ETL are shown in Figure S6 (Supporting Information) and the device performance parameters are summarized in Table S2 (Supporting Information). Incorporation of PBDTT-TT-TEG into the active layer, PCE has risen from 2.00% to 4.92%, indicating the successfully interfacial modification for hole transport. Surprisingly, the best doping concentration of self-organized PBDTT-TT-TEG is not the value of fully coverage of PBDTT-TT-TEG on the surface of active layer, but is a much lower concentration of 3 wt%. The phenomenon can be explained by the surface morphology of PBDTTT-C-T:$PC_{70}BM$:PBDTT-TT-TEG film measured by atomic force microscopy in Figure S7 (Supporting Information). With the content of PBDTT-TT-TEG increasing, the BHJ surface is getting rougher together with some gradually generated aggregations on surface, which may hamper the efficient charge transport at anode interface. Therefore, a complete coverage of PBDTT-TT-TEG layer on top of BHJ surface did not improve the device performance, but delivered a decline of efficiency induced by the undesired aggregation of the TEG. Moreover, the slow drying process has played a crucial role in the formation of this self-organized HTL. In the XPS profiles (Figure S8, Supporting Information), the fast-dried PBDTTT-C-T:$PC_{70}BM$:PBDTT-TT-TEG blend which was achieved by vaporizing the solvent under high vacuum condition only exhibits 30% amounts of O atom on the film surface compared to the slow-dried film, manifesting that only slow vaporizing of solvent can achieve the spontaneous formation of the PBDTT-TT-TEG HTL.[70] Hence the device with incompletely formed HTL by fast drying only obtained a PCE of 2.33% (Table S2 and Figure S8, Supporting Information).

Since the optimized PBDTT-TT-TEG HTL is not a completely covered layer on the active layer, another solution processed WO_3 (sWO_3) HTL is introduced into this I-PSCs to compensate the inadequacy. The solution processed sWO_3 is prepared by tungsten(V) ethoxide ($W(OEt)_5$) or tungsten(VI) ethoxide ($W(OEt)_6$) precursor spin-coated from ethanol solution on surface of BHJ surface under ambient conditions [71] The XPS spectra of PBDTTT-C-T:$PC_{70}BM$/sWO_3 are showed in Figure S9 (Supporting Information), which reveals that the WO_3 layer is successfully formed after deposition the precursor solution on the surface.[71,72] The calculated W:O ratio is 1:2.987 for WO_3 from $W(OEt)_5$ and 1:3.085 for WO_3 from $W(OEt)_6$, which matches well with the stoichiometric composition of WO_3. In comparison with the reference I-PSCs with hydrophilic PEDOT:PSS HTL, WO_3 HTL endows the device Device A (PBDTTT-C-T:$PC_{70}BM$) and Device D (P3HT:PCBM) with a higher efficiency (**Table 2**, Figure S10, Supporting Information), due to the good light reflection[73] and more hydrophobic nature that can form a relatively homogeneous layer on the BHJ layer. For the solution processed WO_3 HTLs, the I-PSCs with

WO_3 from $W(OEt)_6$ receives a better efficiency than that from $W(OEt)_5$, because the conversion of $W(OEt)_5$ to WO_3 under the ambient conditions for 30 min may cause the degradation of device performance (**Figure 3**).

Compared with WO_3 and PBDTT-TT-TEG, the PBDTT-TT-TEG/WO_3 bilayer modified electrode shows a notably reduced WF of 5.12 eV, as revealed by UPS spectra (Figure 2, Figure S11, Supporting Information). Therefore, a large V_{OC} from the inverted PSCs with the bilayer HTL is anticipated. The optimized solution processed I-PSCs ITO/PFN-CbpSO/PBDTTT-C-T:$PC_{70}BM$/HTL/Ag (Device B) with bilayer HTL of PBDTT-TT-TEG/sWO_3 achieved an average PCE of 7.51% with a best PCE of 7.82% (with V_{OC} of 0.765 V, J_{SC} of 15.94 mA cm^{-2} and FF of 64.2%) (Table 1 and Figure 2). However, the devices only with monolayer HTL show the inferior PCEs (average values) of 6.44% for sWO_3/Ag, and 4.34% for PBDTT-TT-TEG/Ag. The improved performance is ascribed to the enhance V_{OC}, J_{SC} and relatively high FF.

Figure 3 is the *J–V* characteristics of the device A without the self-organized PBDTT-TT-TEG layer. Generally, evaporated WO_3 as HTL can perform better in PSCs than solution processed WO_3, which also happened in the cases of Device A and Device D (Figure S10, Supporting Information), due to the homogeneously ultra thin film without defects. However, for Device B, after combination of PBDTT-TT-TEG and sWO_3, the bilayer PBDTT-TT-TEG/sWO_3 HTL with ≈ 15 nm thickness gains a comparable PCE of 7.82% to eWO_3 monolayer HTL (7.96%) with ≈ 10 nm thickness (Figure 3). The remarkable improved average J_{sc} (15.2 mA cm^{-2}) and FF (64.2%) of solution processed HTL based device are the almost identical value to those with eWO_3 HTL (15.3 mA cm^{-2} and 64.4%). We can draw a conclusion that the PBDTT-TT-TEG can not only act as a HTL, but also facilitate the deposition of the ethanol solution of WO_3 precursor on the active layer and enhance the compatibility between the active layer and WO_3, which can be revealed by increased surface wettability of the active layer with water contact angle surface converting from 97° to 82° and the rougher surface of PBDTT-TT-TEG incorporated active layer for a better interfacial adhesion (Figures S4,S7, Supporting Information).[74] As a result, the optimized I-PSCs with the CPE-ILC modified cathode and PBDTT-TT-TEG/WO_3 modified anode could promote better energy alignments at both anode/active layer and cathode/active layer interfaces. It is worthy to note that the respectable device efficiency of 7.82% is obtained from solution-processed I-PSCs with all the layers (except for electrodes) deposited at gentle room temperature, which is compatible for large-scale roll-to-roll technology.

For further enhancement of PCE, optimization on ETL was performed by combination of the n-type MO with CPE into the devices.[75] The conduction band energy of ZnO is well matched with the electron transport energy of fullerene acceptors and its deep valence band energy can also effectively block holes, the n-type and transparent ZnO is thus widely used as ETL in PSC. In our previous study, it was demonstrated that due to the interaction between the CPE and ZnO, combination of CPE and metal oxides as ETL could achieve better band alignment at PCBM/cathode interface and more compatible interaction at ZnO/active layer interface, consequently delivering remarkable improvement in PCE and stability of device.[76] Therefore, the devices with ZnO/CPE bilayer as ETL were fabricated. Device C with the configuration of ITO/ETL/PBDTTT-C-T:$PC_{70}BM$/PBDTT-TT-TEG/WO_3/Ag based on different solution processed ZnO/CPE bilayer ETLs are fabricated, and the related performance are provided in Table 1 and Figure 3. As expected, with relatively hydrophobic CPE-ILC deposited on the surface of solution processed ZnO, the intimate contact and liquid crystal-induced dipole orientation at the ZnO/PFN-CbpSO interface lead to an optimized device efficiency over 8%, which is higher

Table 2. Summary of the photovoltaic performance of P3HT:$PC_{60}BM$ solar cells with various interlayer.

Device[a)]	HTL	V_{OC} [V]	J_{SC} [mA cm^{-2}]	FF [%]	average PCE [%][e)]	best PCE [%]	R_s [Ω cm^2]	R_{sh} [Ω cm^2]
D	none	0.54	7.27	50.1	1.97	2.04	2.42	392
D	PEDOT:PSS	0.61	9.05	55.5	3.06	3.14	6.60	549
D	sWO_3[c)]	0.62	9.16	61.8	3.51	3.67	32.5	428
D	**sWO_3[d)]**	**0.63**	**9.18**	**61.8**	**3.57**	**3.69**	**14.5**	**448**
D	eWO_3	0.63	9.43	67.5	4.01	4.15	0.92	683
E control[b)]	none	0.54	6.56	56.7	2.01	2.13	2.12	696
E	none	0.58	8.10	57.3	2.69	2.81	4.52	535
E	PEDOT:PSS	0.62	9.09	55.2	3.11	3.20	4.92	689
E	sWO_3[c)]	0.62	9.36	64.0	3.71	3.87	30.9	407
E	sWO_3[d)]	0.63	9.38	64.5	3.81	3.97	35.0	525
E	eWO_3	0.64	9.91	68.4	4.34	4.52	2.57	1015

[a)]Device D: glass/ITO/PFN-CbpSO/P3HT:$PC_{60}BM$ (1:1 w/w, 180–200 nm)/HTL/Ag (90 nm) and Device E: glass/ITO/ZnO/PFN-CbpSO/P3HT:$PC_{60}BM$/HTL/Ag. [b)]Device configuration: glass/ITO/ZnO/P3HT:$PC_{60}BM$/HTL/Ag. [c)]The WO_3 fabricated from $W(EtO)_5$. [d)]The WO_3 fabricated from $W(EtO)_6$. [e)]All the PCE were averaged over 5 cells. The bold value is the best performance for the room temperature fabricated devices with solution processed electrode interlayer.

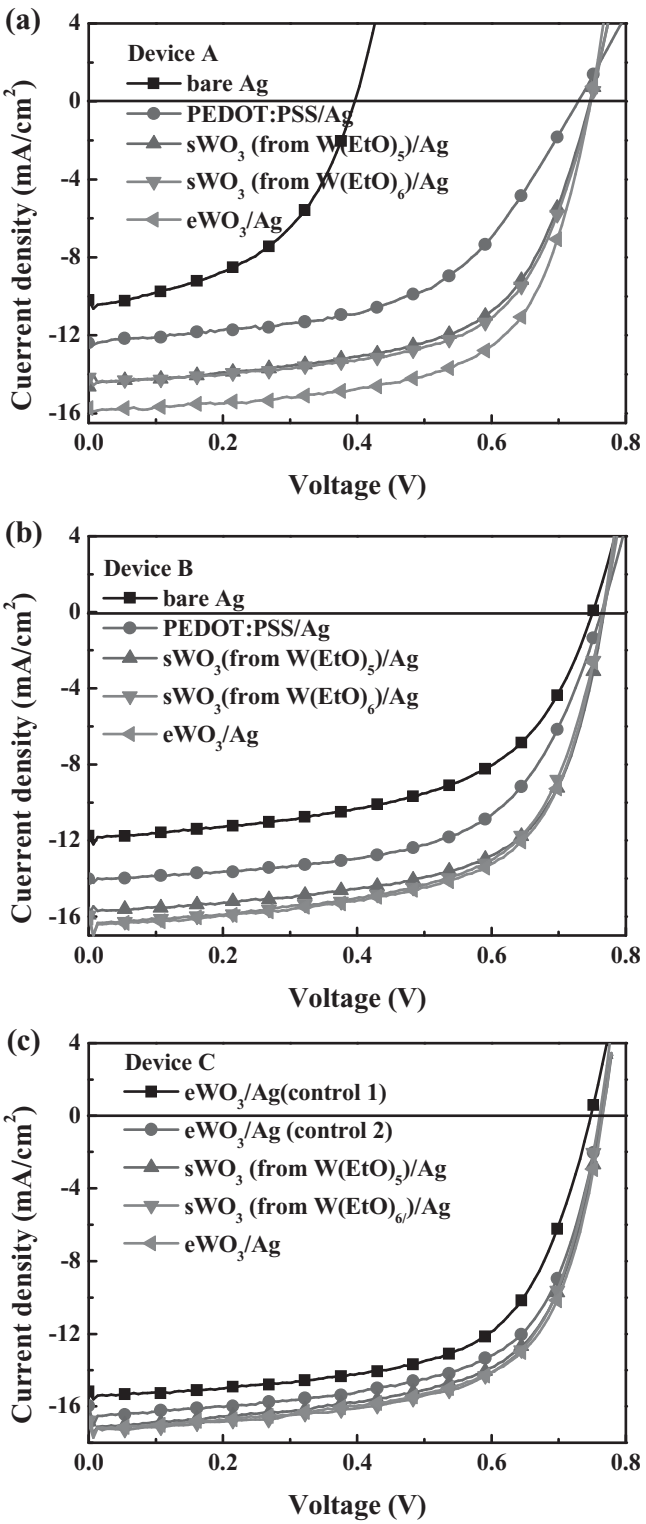

Figure 3. *J–V* characteristics of a) Device A, b) Device B, and c) Device C comprising different HTL materials. (Device A: ITO/PFN-CbpSO/PBDTTT-C-T:$PC_{70}BM$/HTL/Ag; Device B: ITO/PFN-CbpSO/PBDTTT-C-T:$PC_{70}BM$/PBDTT-TT-TEG/HTL/Ag; Device C: ITO/ZnO/PFN-CbpSO/PBDTTT-C-T:$PC_{70}BM$:PBDTT-TT-TEG/HTL/Ag).

than the devices based on bare ZnO (6.92%, Device C, control 1) and ZnO/PFN-Br ETL (7.57%, Devie C, control 2). Note that the device based on solution processed ZnO/PFN-CbpSO bilayer ETL and PBDTT-TT-TEG/sWO_3 bilayer HTL achieves a notable PCE of 8.49% with a further improved J_{SC} of 16.2 mA cm^{-2} and FF of 65.3% with respect to the corresponding Device B without ZnO. To the best of our knowledge, this is the best PCE value for PBDTTT-C-T:$PC_{70}BM$-based solar cells with solution processed interlayers reported to date. Improved PCE, J_{SC}, and FF is correlated to the dramatically enhanced R_{sh} of 4889 Ω cm^2. Also, the P3HT:PCBM-based I-PSCs with the ZnO/CPE-ILC ETL give rise to the performance improvement (Device E, Table 2). Similarly to the case in Device B, replacing sWO_3 to eWO_3 does not bring an obvious change on the all performance parameters, but only obtains a slightly improved average PCE of 8.21% with the best efficiency of 8.53%. This result confirms again that PBDTT-TT-TEG/sWO_3 is an excellent HTL for high performance PSCs and can replace the evaporated WO_3 to meet the printing requirement.

Figure 4 compares the external quantum efficiency (EQE) spectra of the solution processed PBDTTT-C-T:$PC_{70}BM$ I-PSCs with various HTLs. Compared with the devices without HTL and with PEDOT:PSS, the I-PSCs with sWO_3 shows an enhanced response from 320 to 390 nm, originating from the enhanced light absorption caused by the light reflection from MO.[73] The Device A only with WO_3 HTL exhibits a low EQE response, associated with a low J_{SC} of ≈14 mA cm^{-2}. Incorporation of PBDTT-TT-TEG/eWO_3 into the solution processed Device B with the best performance of 7.82% induces a high EQE response over 55% from 420 to 730 nm, with a maximum value of 69.2% at 460 nm. Moreover, the Device C fabricated by all the optimized ETL and HTL receives a maximum EQE response of 76.3% at 460 nm. In addition, expect for Device A without incorporation of TEG-capped PBDTT-TT-TEG, the Device B and C with PBDTT-TT-TEG/sWO_3 or PBDTT-TT-TEG/eWO_3 has identical EQE responses (Figure S12, Supporting Information), which is in agreement with the same J_{SC} values. All J_{SC} values calculated by EQE are listed in Table S3 (Supporting Information), which indicates that the J_{SC} error between the values form *J–V* curves and those calculated by EQE is less than 4%.

Beyond the device efficiency improvement and the solution processibility in room temperature, enhanced device stability from the optimized interfacial layers was also observed in the solution processed devices. **Figure 5** compares the air stability of devices with different electrode interlayers. Devices without encapsulations were placed in air (humidity: ≈55%; temperature: ≈25 °C) in the dark for several days before measurements. The Device A with ETL of PFN-Br decrease 35% PCE value after constant exposure in air for 60 days. In contrast, the Device A with PFN-CbpSO as cathode interlayer has retained 84% efficiency after 8 weeks exposure in ambient. The relatively weak hygroscopicity of the CPE-ILC complex with ILC-packed non-polar side chain is beneficial for slowing down the degradation of devices. Similarly, compared with traditional HTL PEDOT:PSS with hygroscopicity and acidity, the more hydrophobic nature of WO_3 can also enhance the

device immunity to moisture. As shown in Figure 5, Device B with PBDTT-TT-TEG/sWO_3 HTL shows much higher stability than the one with PEDOT:PSS. The I-PSC ITO/PFN-CbpSO/PBDTTT-C-T:$PC_{70}BM$:PBDTT-TT-TEG/sWO_3/Ag with the best efficiency of 7.82% can still maintain 85% of initial value after 56 days in air. The *J–V* characteristics and device parameters values of this long-term stable device as a function of time can be seen in Figure S13. Although the device stability is measured in the dark, and it is not the operational lifetime, but the long shelf-lifetime also suggests that the I-PSCs with the moisture-resistant CPE-ILC and sWO_3 could act as an encapsulation at both bottom and top side to achieve superior air stability.

3. Conclusions

In conclusion, we have developed a room temperature solution fabricated inverted PSC with high efficiency, solution processibility and long-term air stability. Comparing with the pure CPE PFN-Br, the novel self-assembled CPE-ILC complex as ETL improves the compatibility with hydrophobic active layer and the dipole orientation at cathode interface. The polymer PBDTT-TT-TEG with TEG-substituted side chain doped in active layer spontaneously forms a buffer layer at anode. The interfacial dipole induced by TEG side chain efficiently shifts the WF of Ag electrode and the TEG-aggregated BHJ surface is liable for adhesion of the solution processed WO_3. The I-PSCs with the CPE-ILC as ETL and PBDTT-TT-TEG/WO_3 as HTL can achieve energy alignment at both electrodes, which is attributed to the WF reduction at cathode and WF elevation at anode. This room temperature solution fabricated device ITO/PFN-CbpSO/PBDTTT-C-T:$PC_{70}BM$/PBDTT-TT-TEG/sWO_3/Ag achieves an optimized PCE of 7.82%, which is comparable to performance of the corresponding device with evaporated WO_3. The device performance was further improved by introduction of ZnO into cathode interlayer. A higher PCE of 8.5% is obtained from the solution processed device with the configuration of ITO/ZnO/PFN-CbpSO/PBDTTT-C-T:$PC_{70}BM$/PBDTT-TT-TEG/sWO_3/Ag. Moreover, the moisture-resistant property of both CPE-ILC and sWO_3 endows the device with good stability in air. This device has merged the properties of high efficiency, long-term air stability and solution processibility together, which is anticipated to be used for fabricating flexible or large scale devices.

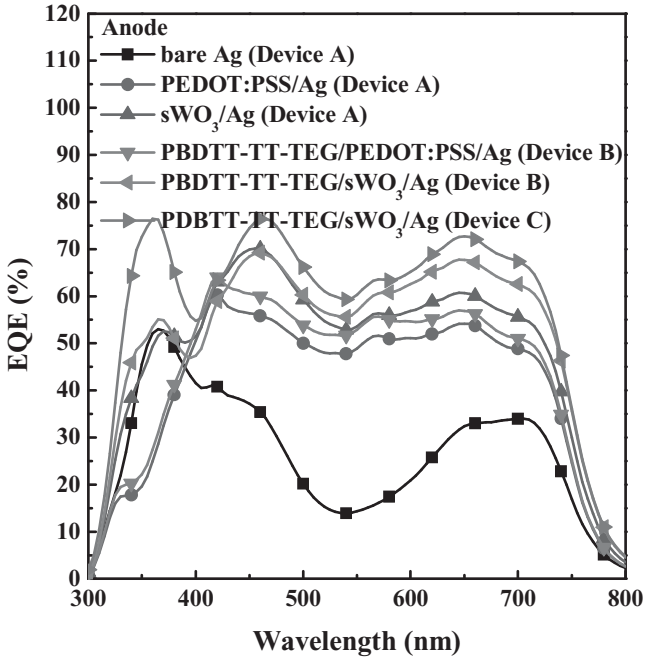

Figure 4. EQE spectra of the PBDTTT-C-T:$PC_{70}BM$ I-PSCs with various HTL materials.

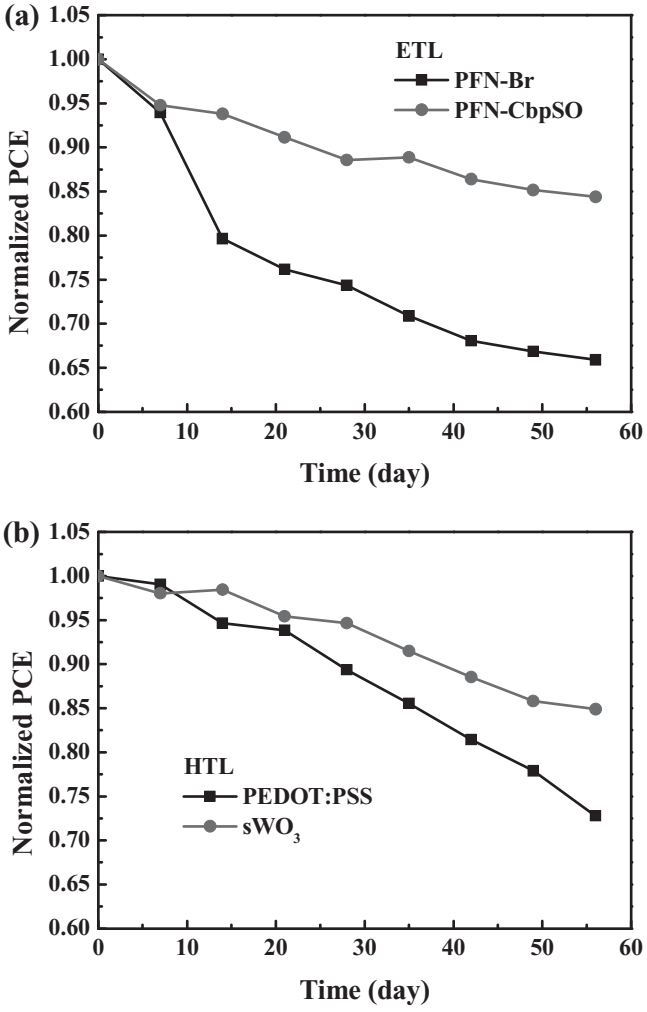

Figure 5. Normalized PCE decay of I-PSCs a) ITO/ETL/PBDTTT-C-T:$PC_{70}BM$/eWO_3/Ag using PFNBr or PFN-CbpSO as ETL, b) ITO/PFN-CbpSO/PBDTTT-C-T:$PC_{70}BM$:PBDTT-TT-TEG/HTL/Ag using PEDOT:PSS or solution processed WO_3 as HTL at ambient conditions.

4. Experimental Section

Preparation of PFN-CbpSO Complex: PFN-Br and CbpSO-Na were dissolved in water in the 1:2 stoichiometric molar ratio and stirred for several hours to form an intensive mixed solution. Then the formed complex precipitated in water during this period. The precipitation was collected by filtration and washed three times with de-ionized water to remove the residual water-soluble CPE, ILC and the NaBr salts. Finally,

the precipitate was dried under vacuum overnight to yield the purified complex. The molar ratio of the two counterparts PFN to CbpSO in the complex was verified by the integrated area of resonance peaks at ≈2.93 ppm and ≈3.98 ppm in the ^{1}H NMR spectrum, corresponding to the protons in N atom from PFN (18H) and in alkyl chain from CbpSO (4H), respectively (see Figure S1, Supporting Information).

Synthesis of PBDTT-TT-TEG: This polymer PBDTT-TT-TEG was synthesized according to the reported literatures.[63,69] General method of polymerization by Stille coupling. The 2,6-Bis(trimethyltin)-4,8-bis(5-(2-ethylhexyl)thiophen-2-yl)benzo[1,2-b:4,5-b′]dithiophene (BDTT) monomer (0.5 mmol) and the 4,6-Dibromo-thieno[3,4-b]thiophene-2-carboxylic acid 2-[2-(2-methoxy-ethoxy)-ethoxy]-ethyl ester (TT-TEG) monomer (0.5 mmol) were mixed in toluene (10 mL) and DMF (2 mL). After being purged with argon for 5 min, [$Pd(PPh_3)_4$] (30 mg) was added as the catalyst, and the mixture was then purged with argon for 25 min. The reaction mixture was stirred and heated to reflux for 16 h. Then the reaction mixture was cooled to room temperature, and the polymer was precipitated by addition of methanol (50 mL), filtered through a Soxhlet thimble. The precipitate was then subjected to Soxhlet extraction with methanol, hexanes, and chloroform. The polymer was recovered as solid from the chloroform fraction by precipitation from methanol (221 mg, 52%). ^{1}H NMR (δ, $CDCl_3$-d_1): 7.66–6.69 (m, 7H), 4.42–3.24 (br, 11H), 2.51–0.96(m, 34H).

Fabrication of PSCs: In the inverted device fabrication process, ITO-coated glass substrates were first cleaned by ultrasonic agitation in acetone, detergent, deionized water, and isopropanol sequentially, followed by UV treatment for 20 min. PFN-CbpSO interlayer was was dissolved in methanol with a concentration of 0.2 wt% and the solution was spin cast on the ITO at a speed of 5000 rpm for 40 s. The film was then treated by oxygen plasma cleaner for 5 min. The sol-gel derived ZnO film was placed on the top of ITO glass using the reported method.[47] The PBDTTT-C-T (10 mg mL^{-1}), PBDTT-TT-TEG (3 mg mL^{-1}) and $PC_{70}BM$ (15 mg mL^{-1}) were dissolved in 1 mL o-dichlorobenzene (ODCB) with 3% diiodooctane, and the blend was coated onto the ETL at a speed of 900 rpm for 1 min to form a BHJ layer. For the PSCs based on P3HT:PCBM, the active layer was formed by spin-coating ODCB solution containing 20 mg mL^{-1} P3HT/PCBM (1:1 w/w) at 800 rpm. An ethanol diluted $W(OEt)_5$ or $W(OEt)_6$ precursor solution (approximately 3 mg·mL^{-1}) was then deposited on the top of active layer, and subsequently stored at room temperature either under ambient or under inert conditions to allow for hydrolytic conversion of the precursor (30 min). The devices were completed by evaporating Ag or eWO_3/Ag anode with an area of 4 mm^2 as defined by masks.

Characterization of PSCs: The light source was calibrated by using silicon reference cells with an AM 1.5 Global solar simulator with an intensity of 100 mW/cm^2. The current–voltage (*J–V*) characteristics were recorded using Keithley 2400 Source Meter(Abet Solar Simulator Sun2000). All the measurements were performed under ambient atmosphere at room temperature. The EQE was measured under monochromatic illumination (Oriel Cornerstone 260 1/4 m monochromator equipped with Oriel 70613NS QTH lamp), and the calibration of the incident light was performed with a monocrystalline silicon diode.

Work Function Measurements by UPS: The ITO, ITO/PFN-Br and ITO/PFN-CbpSO samples were prepared by spin coating the solution of CPE on the pre-cleaned glass/ITO surface and without further treatment. The Ag, PBDTT-TT-TEG/Ag, WO_3/Ag and PBDTT-TT-TEG/WO_3/Ag samples were prepared on by spin coating the precursor solution on the surface of quartz glass followed by evaporating 5 nm Ag on top of the film. The UPS measurements were carried out in a Thermo-VG Scientific ESCALAB 250 using a He I (21.22 eV) discharge lamp. A bias of –8.0 V was applied to the samples for separation of the sample and the secondary edge for the analyzer.

Supporting Information

Supporting Information is available from the Wiley Online Library or from the author.

Acknowledgements

This work was supported by the National Natural Science Foundation of China (51273088, and 51263016). C.X. and L.C. contributed equally to this work.

Received: December 22, 2013
Revised: February 6, 2014
Published online: March 24, 2014

[1] G. Yu, J. Gao, J. C. Hummelen, F. Wudl, A. J. Heeger, *Science* **1995**, *270*, 1789.
[2] G. Dennler, M. C. Scharber, C. J. Brabec, *Adv. Mater.* **2009**, *21*, 1323.
[3] G. Li, R. Zhu, Y. Yang, *Nat. Photonics* **2012**, *6*, 153.
[4] M. Jorgensen, K. Norrman, S. A. Gevorgyan, T. Tromholt, B. Andreasen, F. C. Krebs, *Adv. Mater.* **2012**, *24*, 580.
[5] M. Jørgensen, K. Norrman, F. C. Krebs, *Sol. Energy Mater. Sol. Cells* **2008**, *92*, 686.
[6] J. You, L. Dou, K. Yoshimura, T. Kato, K. Ohya, T. Moriarty, K. Emery, C. C. Chen, J. Gao, G. Li, Y. Yang, *Nat. Commun.* **2013**, *4*, 1446.
[7] J. You, C. C. Chen, Z. Hong, K. Yoshimura, K. Ohya, R. Xu, S. Ye, J. Gao, G. Li, Y. Yang, *Adv. Mater.* **2013**, *25*, 3973.
[8] H.-Y. Chen, J. Hou, S. Zhang, Y. Liang, G. Yang, Y. Yang, L. Yu, Y. Wu, G. Li, *Nat. Photonics* **2009**, *3*, 649.
[9] P. M. Beaujuge, J. M. Frechet, *J. Am. Chem. Soc.* **2011**, *133*, 20009.
[10] Y. Li, *Acc. Chem. Res.* **2012**, *45*, 723.
[11] H.-L. Yip, A. K. Y. Jen, *Energy Environ. Sci.* **2012**, *5*, 5994.
[12] T. Ameri, N. Li, C. J. Brabec, *Energy Environ. Sci.* **2013**, *6*, 2390.
[13] R. Po, C. Carbonera, A. Bernardi, N. Camaioni, *Energy Environ. Sci.* **2011**, *4*, 285.
[14] Z. He, C. Zhong, S. Su, M. Xu, H. Wu, Y. Cao, *Nat. Photonics* **2012**, *6*, 591.
[15] G. Li, C. W. Chu, V. Shrotriya, J. Huang, Y. Yang, *Appl. Phys. Lett.* **2006**, *88*, 253503.
[16] M. Glatthaar, M. Niggemann, B. Zimmermann, P. Lewer, M. Riede, A. Hinsch, J. Luther, *Thin Solid Films* **2005**, *491*, 298.
[17] B. J. Kim, Y. Miyamoto, B. Ma, J. M. J. Fréchet, *Adv. Funct. Mater.* **2009**, *19*, 2273.
[18] F. C. Krebs, *Org. Electron.* **2009**, *10*, 761.
[19] F. C. Krebs, S. A. Gevorgyan, J. Alstrup, *J. Mater. Chem.* **2009**, *19*, 5442.
[20] J. A. Hauch, P. Schilinsky, S. A. Choulis, R. Childers, M. Biele, C. J. Brabec, *Sol. Energy Mater. Sol. Cells* **2008**, *92*, 727.
[21] D. M. Tanenbaum, H. F. Dam, R. Rösch, M. Jørgensen, H. Hoppe, F. C. Krebs, *Sol. Energy Mater. Sol. Cells* **2012**, *97*, 157.
[22] E. Voroshazi, B. Verreet, A. Buri, R. Müller, D. Di Nuzzo, P. Heremans, *Org. Electron.* **2011**, *12*, 736.
[23] K. Norrman, S. A. Gevorgyan, F. C. Krebs, *ACS Appl. Mater. Interfaces* **2009**, *1*, 102.
[24] J. Meyer, R. Khalandovsky, P. Gorrn, A. Kahn, *Adv. Mater.* **2011**, *23*, 70.
[25] H. Béa, M. Bibes, M. Sirena, G. Herranz, K. Bouzehouane, E. Jacquet, S. Fusil, P. Paruch, M. Dawber, J. P. Contour, A. Barthélémy, *Appl. Phys. Lett.* **2006**, *88*, 062502.
[26] F. Liu, S. Shao, X. Guo, Y. Zhao, Z. Xie, *Sol. Energy Mater. Sol. Cells* **2010**, *94*, 842.
[27] S. Murase, Y. Yang, *Adv. Mater.* **2012**, *24*, 2459.
[28] T. Stubhan, T. Ameri, M. Salinas, J. Krantz, F. Machui, M. Halik, C. J. Brabec, *Appl. Phys. Lett.* **2011**, *98*, 253308.
[29] F. Xie, W. C. Choy, C. Wang, X. Li, S. Zhang, J. Hou, *Adv. Mater.* **2013**, *25*, 2051.
[30] G. Terán-Escobar, J. Pampel, J. M. Caicedo, M. Lira-Cantú, *Energy Environ. Sci.* **2013**, *6*, 3088.

[31] H.-Q. Wang, N. Li, N. S. Guldal, C. J. Brabec, *Org. Electron.* **2012**, *13*, 3014.
[32] M. Hajzeri, A. Šurca Vuk, L. Slemenik Perše, M. Čolović, B. Herbig, U. Posset, M. Kržmanc, B. Orel, *Sol. Energy Mater. Sol. Cells* **2012**, *99*, 62.
[33] M. D. Irwin, J. D. Servaites, D. B. Buchholz, B. J. Leever, J. Liu, J. D. Emery, M. Zhang, J.-H. Song, M. F. Durstock, A. J. Freeman, M. J. Bedzyk, M. C. Hersam, R. P. H. Chang, M. A. Ratner, T. J. Marks, *Chem. Mater.* **2011**, *23*, 2218.
[34] K. X. Steirer, J. P. Chesin, N. E. Widjonarko, J. J. Berry, A. Miedaner, D. S. Ginley, D. C. Olson, *Org. Electron.* **2010**, *11*, 1414.
[35] K. X. Steirer, P. F. Ndione, N. E. Widjonarko, M. T. Lloyd, J. Meyer, E. L. Ratcliff, A. Kahn, N. R. Armstrong, C. J. Curtis, D. S. Ginley, J. J. Berry, D. C. Olson, *Adv. Energy Mater.* **2011**, *1*, 813.
[36] L. Zuo, X. Jiang, L. Yang, M. Xu, Y. Nan, Q. Yan, H. Chen, *Appl. Phys. Lett.* **2011**, *99*, 183306.
[37] T. Stubhan, N. Li, N. A. Luechinger, S. C. Halim, G. J. Matt, C. J. Brabec, *Adv. Energy Mater.* **2012**, *2*, 1433.
[38] S. B. Lee, J. Ho Beak, B. h. Kang, K.-Y. Dong, Y.-Y. Yu, Y. Doo Lee, B.-K. Ju, *Sol. Energy Mater. Sol. Cells* **2013**, *117*, 203.
[39] N. Li, T. Stubhan, N. A. Luechinger, S. C. Halim, G. J. Matt, T. Ameri, C. J. Brabec, *Org. Electron.* **2012**, *13*, 2479.
[40] Z. Tan, L. Li, C. Cui, Y. Ding, Q. Xu, S. Li, D. Qian, Y. Li, *J. Phys. Chem. C* **2012**, *116*, 18626.
[41] M. Ghasemi Varnamkhasti, H. R. Fallah, M. Mostajaboddavati, R. Ghasemi, A. Hassanzadeh, *Sol. Energy Mater. Sol. Cells* **2012**, *98*, 379.
[42] H. Choi, B. Kim, M. J. Ko, D.-K. Lee, H. Kim, S. H. Kim, K. Kim, *Org. Electron.* **2012**, *13*, 959.
[43] C. Tao, S. Ruan, G. Xie, X. Kong, L. Shen, F. Meng, C. Liu, X. Zhang, W. Dong, W. Chen, *Appl. Phys. Lett.* **2009**, *94*, 043311.
[44] S. Han, W. S. Shin, M. Seo, D. Gupta, S.-J. Moon, S. Yoo, *Org. Electron.* **2009**, *10*, 791.
[45] J. Y. Kim, S. H. Kim, H. H. Lee, K. Lee, W. Ma, X. Gong, A. J. Heeger, *Adv. Mater.* **2006**, *18*, 572.
[46] H. Faber, M. Burkhardt, A. Jedaa, D. Kälblein, H. Klauk, M. Halik, *Adv. Mater.* **2009**, *21*, 3099.
[47] Y. Sun, J. H. Seo, C. J. Takacs, J. Seifter, A. J. Heeger, *Adv. Mater.* **2011**, *23*, 1679.
[48] Z. Chen, H. Zhang, X. Du, X. Cheng, X. Chen, Y. Jiang, B. Yang, *Energy Environ. Sci.* **2013**, *6*, 1597.
[49] Z. Chen, H. Zhang, W. Yu, Z. Li, J. Hou, H. Wei, B. Yang, *Adv. Energy Mater.* **2013**, *3*, 433.
[50] X. Bulliard, S.-G. Ihn, S. Yun, Y. Kim, D. Choi, J.-Y. Choi, M. Kim, M. Sim, J.-H. Park, W. Choi, K. Cho, *Adv. Funct. Mater.* **2010**, *20*, 4381.
[51] J. H. Seo, A. Gutacker, Y. Sun, H. Wu, F. Huang, Y. Cao, U. Scherf, A. J. Heeger, G. C. Bazan, *J. Am. Chem. Soc.* **2011**, *133*, 8416.
[52] C. Duan, K. Zhang, C. Zhong, F. Huang, Y. Cao, *Chem. Soc. Rev.* **2013**, *42*, 9071.
[53] S. H. Liao, Y. L. Li, T. H. Jen, Y. S. Cheng, S. A. Chen, *J. Am. Chem. Soc.* **2012**, *134*, 14271.
[54] H. Kang, S. Hong, J. Lee, K. Lee, *Adv. Mater.* **2012**, *24*, 3005.
[55] Y. Zhou, C. Fuentes-Hernandez, J. Shim, J. Meyer, A. J. Giordano, H. Li, P. Winget, T. Papadopoulos, H. Cheun, J. Kim, M. Fenoll, A. Dindar, W. Haske, E. Najafabadi, T. M. Khan, H. Sojoudi, S. Barlow, S. Graham, J. L. Bredas, S. R. Marder, A. Kahn, B. Kippelen, *Science* **2012**, *336*, 327.
[56] A. K. Kyaw, D. H. Wang, V. Gupta, J. Zhang, S. Chand, G. C. Bazan, A. J. Heeger, *Adv. Mater.* **2013**, *25*, 2397.
[57] J. W. Jung, J. W. Jo, W. H. Jo, *Adv. Mater.* **2011**, *23*, 1782.
[58] C.-Z. Li, C.-C. Chueh, H.-L. Yip, K. M. O'Malley, W.-C. Chen, A. K. Y. Jen, *J. Mater. Chem.* **2012**, *22*, 8574.
[59] C. Duan, C. Zhong, C. Liu, F. Huang, Y. Cao, *Chem. Mater.* **2012**, *24*, 1682.
[60] C.-H. Hsieh, Y.-J. Cheng, P.-J. Li, C.-H. Chen, M. Dubosc, R.-M. Liang, C.-S. Hsu, *J. Am. Chem. Soc.* **2010**, *132*, 4887.
[61] Y.-J. Cheng, C.-H. Hsieh, Y. He, C.-S. Hsu, Y. Li, *J. Am. Chem. Soc.* **2010**, *132*, 17381.
[62] Y.-J. Cheng, F.-Y. Cao, W.-C. Lin, C.-H. Chen, C.-H. Hsieh, *Chem. Mater.* **2011**, *23*, 1512.
[63] L. Huo, S. Zhang, X. Guo, F. Xu, Y. Li, J. Hou, *Angew. Chem. Int. Ed.* **2011**, *50*, 9697.
[64] L. Chen, C. Xie, Y. Chen, *Org. Electron.* **2013**, *14*, 1551.
[65] Y.-M. Chang, R. Zhu, E. Richard, C.-C. Chen, G. Li, Y. Yang, *Adv. Funct. Mater.* **2012**, *22*, 3284.
[66] R. Schlaf, H. Murata, Z. H. Kafafi, *J. Electron Spectrosc. Relat. Phenom.* **2001**, *120*, 149.
[67] S. Gutmann, M. u. A. Wolak, M. Conrad, M. M. Beerbom, R. Schlaf, *J. Appl. Phys.* **2011**, *109*, 113719.
[68] F.-C. Chen, S.-C. Chien, *J. Mater. Chem.* **2009**, *19*, 6865.
[69] Y. Liang, S. Xiao, D. Feng, L. Yu, *J. Phys. Chem. C* **2008**, *112*, 7866.
[70] G. Li, V. Shrotriya, J. Huang, Y. Yao, T. Moriarty, K. Emery, Y. Yang, *Nat. Mater.* **2005**, *4*, 864.
[71] S. Hofle, M. Bruns, S. Strassle, C. Feldmann, U. Lemmer, A. Colsmann, *Adv. Mater.* **2013**, *25*, 4113.
[72] R. Hock, T. Mayer, W. Jaegermann, *J. Phys. Chem. C* **2012**, *116*, 18146.
[73] A. K. Kyaw, D. H. Wang, D. Wynands, J. Zhang, T. Q. Nguyen, G. C. Bazan, A. J. Heeger, *Nano. Lett.* **2013**, *13*, 3796.
[74] W. Ma, C. Yang, X. Gong, K. Lee, A. J. Heeger, *Adv. Funct. Mater.* **2005**, *15*, 1617.
[75] T. Yang, M. Wang, C. Duan, X. Hu, L. Huang, J. Peng, F. Huang, X. Gong, *Energy Environ. Sci.* **2012**, *5*, 8208.
[76] C. Xie, L. Chen, Y. Chen, *J. Phys. Chem. C* **2013**, *117*, 24804.